Astronomy & Astrophysics

Reaction rate uncertainties and the operation of the NeNa and MgAl chains during HBB in intermediate-mass AGB stars[*]

R. G. Izzard[1,**], M. Lugaro[1,**], A. I. Karakas[2,***], C. Iliadis[3,4], and M. van Raai[1]

[1] Sterrekundig Instituut, University of Utrecht, Postbus 80000 3508 TA Utrecht, The Netherlands
e-mail: [R.G.Izzard;M.Lugaro;raai]@phys.uu.nl
[2] Origins Institute, Department of Physics & Astronomy, McMaster University, Hamilton ON, Canada
e-mail: karakas@physics.mcmaster.ca
[3] Department of Physics and Astronomy, University of North Carolina, Chapel Hill, NC 27599-3255, USA
e-mail: iliadis@unc.edu
[4] Triangle Universities Nuclear Laboratory, PO Box 90308, Durham, NC 27708-0308, USA

ABSTRACT

Context. We test the effect of proton-capture reaction rate uncertainties on the abundances of the Ne, Na, Mg and Al isotopes processed by the NeNa and MgAl chains during hot bottom burning (HBB) in asymptotic giant branch (AGB) stars of intermediate mass between 4 and 6 $M_\odot$ and metallicities between $Z = 0.0001$ and 0.02.
Aims. We provide uncertainty ranges for the AGB stellar yields, for inclusion in galactic chemical evolution models, and indicate which reaction rates are most important and should be better determined.
Methods. We use a fast synthetic algorithm based on detailed AGB models. We run a large number of stellar models, varying one reaction rate per time for a very fine grid of values, as well as all reactions simultaneously.
Results. We show that there are uncertainties in the yields of all the Ne, Na, Mg and Al isotopes due to uncertain proton-capture reaction rates. The most uncertain yields are those of ^{26}Al and ^{23}Na (variations of two orders of magnitude), ^{24}Mg and ^{27}Al (variations of more than one order of magnitude), ^{20}Ne and ^{22}Ne (variations between factors 2 and 7). In order to obtain more reliable Ne, Na, Mg and Al yields from IM-AGB stars the rates that require more accurate determination are: ^{22}Ne$(p,\gamma)^{23}$Na, ^{23}Na$(p,\gamma)^{24}$Mg, ^{25}Mg$(p,\gamma)^{26}$Al, ^{26}Mg$(p,\gamma)^{27}$Al and ^{26}Al$(p,\gamma)^{27}$Si.
Conclusions. Detailed galactic chemical evolution models should be constructed to address the impact of our uncertainty ranges on the observational constraints related to HBB nucleosynthesis, such as globular cluster chemical anomalies.

Key words. nuclear reactions, nucleosynthesis, abundances – stars: AGB and post-AGB

1. Introduction

During the asymptotic giant branch (AGB) phase of stars (with initial masses between approximately 1 and 10 $M_\odot$) the abundances of several isotopes are modified via complex nucleosynthetic mechanisms. Hydrogen and helium burning occur alternately in shells in the deep layers of the star and mixing processes collectively known as the third dredge-up (TDU) carry the processed material to the stellar surface. Strong stellar winds eject the envelope of the star into the interstellar medium so that AGB stars contribute to the chemical evolution of galaxies. In AGB stars of masses higher than roughly 4 $M_\odot$ (intermediate mass AGB stars, IM-AGB), H-burning occurs at the base of the convective H-rich envelope and its products are mixed to the surface of the star by convection. This process is called hot-bottom burning (HBB) and involves activation of the CNO, NeNa and MgAl cycles at temperatures between 60 and 100 million degrees. The activation of HBB in IM-AGB stars is validated by

the fact that there appears to be an upper limit for the luminosity of carbon stars, in agreement with the fact that HBB would prevent the more massive AGB stars from becoming carbon rich (Boothroyd et al. 1993).

There are several types of applications for models of IM-AGB stars suffering HBB. Some direct observations of Li, C and the ^{12}C/^{13}C ratios in IM-AGB stars are available, in particular for stars in the Magellanic Clouds (see e.g. Wood et al. 1983, and Plez et al. 1993), but also recently for our Galaxy (García-Hernández et al. 2007). Stellar models are able to explain the fact that the majority of AGB stars of high luminosity are O rich, as well as to reproduce the observed low ^{12}C/^{13}C ratios and high Li abundances (e.g. Boothroyd et al. 1993; and Mazzitelli et al. 1999). More observational evidence of the occurrence of HBB comes from the fact that planetary nebulae of type I, which are believed to come from massive AGBs, have enhanced He and N/O ratios, which can be explained by HBB in their AGB precursors (Peimbert 1980; Pottasch & Bernard-Salas 2006; Stanghellini et al. 2006).

Intermediate-mass AGB stars with HBB are candidates for pollution of globular cluster stars showing anomalies in O, Na, Mg, and Al (see review by Gratton et al. 2004). Moreover, HBB combined with partial He burning and TDU make IM-AGB stars a site of production for at least part of the primary N observed at low metallicities (Spite et al. 2005). The effect of IM-AGB

---

nucleosynthesis on the Mg isotopes has also been studied in relation to the apparent observed variation of the fine structure constant deduced from quasar absorption lines at redshift <2, which also depends on the abundance of the Mg isotopes (Ashenfelter et al. 2004; Fenner et al. 2005). In this case, as well as in the study of abundance anomalies in globular clusters, AGB stellar yields have to be included into galactic chemical evolution (GCE) models in order to produce predictions to compare to the observable data (see e.g. Fenner et al. 2004). Finally, the origin of one meteoritic presolar spinel grain has been attributed to an IM-AGB star, providing the opportunity of studying massive AGBs using presolar grains (Lugaro et al. 2007).

In summary, there are several applications of the study of HBB, however, IM-AGB stellar models and the resulting stellar yields have been calculated so far largely ignoring the effects of reaction-rate uncertainties. Ventura & D'Antona (2005a) have produced two runs of one IM-AGB model using two sets of reaction rates: the old compilation of Caughlan & Fowler (1988) and the new NACRE compilation (Angulo et al 1999). They found that uncertainties in the stellar structure physics, such as the mass-loss rate and the treatment of convection, produce errors in the resulting yields that are much larger than those produced by changing the rate compilation. However, comparing results for two different sets of rates does not exhaust the problem of testing reaction-rate uncertainties. Lugaro et al. (2004) analyzed in detail the uncertainties of reaction rates in relation to the production of fluorine in AGB stars, and also discussed one IM-AGB model. Karakas et al. (2006) produced a detailed analysis of the effect in IM-AGB stars of the uncertainties of the rates for the ^{22}Ne+α reactions, which are responsible for the production of the heavy Mg isotopes during He burning. These authors presented new estimates for such rates, reducing the previous large errors of NACRE to much smaller ranges, and demonstrated that these rates do not constitute a source of uncertainties in IM-AGB models anymore. However, the precision with which the abundances of the Mg, as well as Ne, Na and Al, isotopes in IM-AGB stars can be predicted is still undermined by uncertainties in the proton capture reaction involved in the NeNa and MgAl chains. Ventura & D'Antona (2006) considered in particular the effect of the uncertainties in the rates that produce and destroy ^{23}Na in their $M = 5\,M_\odot$ and $Z = 0.001$ model.

With the present work we attempt to fill the gap in the analysis of uncertainties connected to the yields from IM-AGB stars. Our analysis has two main motivations: we want to provide uncertainties for the stellar yields, for inclusion in GCE models, and we want to indicate which reaction rates require better determination. Our work is targeted specifically at the NeNa and MgAl chains during HBB. The Ne, Na, Mg and Al isotopes are of interest in all the applications of IM-AGB star nucleosynthesis listed above and our calculation tools are most suitable to this problem: we can treat these proton-capture processes in an analytical way and produce a very large number of stars in a reasonable time. It is not possible to perform the same analysis with our method for the CNO cycle because changing the rates in the CNO cycle would affect the stellar structure, i.e. the temperature at the base of the convective envelope and the convection timescale, which are not calculated in our synthetic post-processing but taken from the detailed AGB models.

The present study has been inspired by two previous works aimed at systematically testing the effect of reaction rate uncertainties: the paper on nova nucleosynthesis by Iliadis et al. (2002) and the paper on the oxygen isotopic ratios in red giant stars by Stoesz & Herwig (2003). While Iliadis et al. (2002) could only test one rate at a time, and Stoesz & Herwig (2003)

used a Monte Carlo approach to run the grid of models varying the reaction rates, the method we use is so fast that we can run a large number (typically 10^4) of stellar models varying one reaction at a time for a very fine grid of values, as well as all reactions simultaneously. Still, our models are based on fully-evolved stellar structure models.

The paper is structured as follows: in Sect. 2 we describe our methods and models in detail, in Sect. 3 we list the reaction rates and the uncertainties we have employed. In Sect. 4 we present the results. In Sect. 5 we summarize the results, and present our conclusions.

As a final introductory comment we observe that it is not in our aims to discuss any of the major uncertainties that are still related to the stellar structure of IM-AGB models, such as the mass-loss law, the treatment of convection, and the determination of convective borders. Discussions of these can be found for example in Herwig (2005), Ventura & D'Antona (2005a,b), Karakas et al. (2006), Lugaro et al. (2007). These uncertainties are typically large and difficult to estimate, calling for more work to be done on the physics of AGB models.

2. Methods and models

We use the single and binary synthetic nucleosynthesis model of Izzard et al. (2006, hereafter: the *synthetic* models), where third dredge-up is followed according to the prescriptions of Karakas et al. (2002). The hot bottom burning model is described by Izzard et al. (2004) and updated by Izzard et al. (2006). It approximates HBB in AGB stars by replacing the many burning and mixing cycles of a detailed stellar evolutionary calculation with a single burning and mixing event at each pulse. The third dredge-up, the fraction of the stellar envelope exposed to HBB, and the burning timescale are calibrated to the detailed stellar evolution models of Karakas et al. (2002). The maximum temperature at the base of the convective envelope ($T_{\mathrm{bce}}^{\max}$) and the total amount of third dredge-up ($M_{\mathrm{TDU}}^{\mathrm{tot}}$) obtained from the detailed calculations for all the stellar models considered here are presented in Table 1. The CNO, NeNa and MgAl cycles are followed by analytic solution of the appropriate differential rate equations, which means our synthetic model is both extremely fast and accurate. We follow both the ground and metastable state of ^{26}Al, but it turned out that introducing the metastable state does not alter our results significantly.

The contribution to luminosity or opacity, and hence stellar structure, of the NeNa and MgAl cycles is negligible, so we make the assumption that we can vary the rates of nuclear reactions involving these species without changing the physical parameters of the star such as interpulse periods and the amount of third dredge-up. We could not, for example, change the CNO cycle reaction rates, as these alter the interpulse period and the amount of third dredge-up (Herwig & Austin 2004).

The stellar yields for the Ne, Na, Mg, and Al isotopes calculated by the synthetic models by setting all the reaction rates to their recommended values (see details in Sect. 3 and Table 3) are listed in Table 2. These yields are defined as the total mass ejected of each isotope in solar masses and represent our control values. In the same table we also present the yields from the models of Karakas et al. (2002, hereafter: the *detailed* models) calculated by setting all the reaction rates to the same recommended values used in the synthetic models. Note that initial compositions for the models with metallicity lower than solar are always taken to be scaled solar. IM-AGB stars are important producers of ^{22}Ne, ^{25}Mg, ^{26}Mg and ^{26}Al. The galactic production of α-nuclei ^{20}Ne and ^{24}Mg and that of ^{27}Al is instead

Table 1. Maximum temperature at the base of the convective envelope ($T_{\mathrm{bce}}^{\mathrm{max}}$), and total third dredge-up mass ($M_{\mathrm{TDU}}^{\mathrm{tot}}$) extracted from the detailed calculations for all the models discussed here.

Model(M,Z)	$T_{\mathrm{bce}}^{\mathrm{max}}/10^7$ K	$M_{\mathrm{TDU}}^{\mathrm{tot}}$ ($M_\odot$)
5,0.02	6.26	0.050
6,0.02	8.26	0.058
5,0.008	8.03	0.180
6,0.008	8.90	0.126
5,0.004	8.39	0.225
6,0.004	9.40	0.151
4,0.0001	8.22	0.302
5,0.0001	9.10	0.320
6,0.0001	10.3	0.119

dominated by supernova nucleosynthesis, even if IM-AGB nucleosynthesis can affect the abundances of ^{24}Mg, which can be heavily destroyed in low-metallicity models and of ^{27}Al, which can be slightly produced.

The ratio between the detailed and the synthetic models are typically within a factor of two, except for the isotopes of lowest abundance: ^{21}Ne (ratios up to 4) and ^{26}Al (ratios up to 5.4) and for the $M = 6$ $M_\odot$ and $Z = 0.0001$ model. These differences come up for a number of reasons:

1. In the synthetic models the AGB evolution is followed right to the end, i.e. until the envelope is completely lost, while in the detailed models the AGB evolution is followed up to a point when the code does not converge anymore or when an enormous amount of models has been generated. To calculate the yields it is assumed that the rest of the envelope is ejected with the final computed composition. Hence, more thermal pulses and a longer time for HBB is considered in the calculation of the synthetic yields. In particular, this explains the differences obtained for the $M = 6$ $M_\odot$ and $Z = 0.0001$ model, which are larger than for the other models: in fact, with the detailed models we calculated 106 thermal pulses and then the computation was stopped, however, the total mass of the star was still 5.96 $M_\odot$ at this point of the evolution[1].
2. The effect of the second dredge-up on the elements considered here is not accounted for in the synthetic models.
3. The dredge-up of the thin layer of H-burning ashes in the intershell not engulfed in the thermal pulses is accounted for in the detailed but not in the synthetic models.
4. The $M = 4$ and $M = 5$ $M_\odot$ $Z = 0.0001$ models present degenerate pulses (Frost et al. 1998), which are handled properly by the detailed models but are not included in the synthetic model.
5. Finally, of course, the synthetic algorithm is by its nature approximate.

The relatively small differences between our detailed and synthetic yields are well within stellar model uncertainties and, in many cases, also within reaction rate uncertainties (see Sect. 4).

---

[1] Note that the $M = 6$ $M_\odot$ and $Z = 0.0001$ model has 691 973 evolutionary steps, and it takes almost two weeks to compute the detailed nucleosynthesis on a AMD athlon 3500+ 64bit, ASUS A8V deluxe machine. The $M = 5$ $M_\odot$ and $Z = 0.0001$ model, for which we have calculated 136 thermal pulses with a final envelope mass of 0.76 $M_\odot$, has 1 278 389 evolution models and it takes four weeks to compute the detailed nucleosynthesis. It is clearly not computationally feasible to get to the end of the evolution for the $M = 6$ $M_\odot$ and $Z = 0.0001$ model with the detailed calculations.

In any case, we have tested for the $M = 6$ $M_\odot$ $Z = 0.02$ and $Z = 0.004$ models that the range in the yields derived from the synthetic models by varying the reaction rates within their uncertainties is the same as derived from the detailed models for the important cases of the upper limits of the ^{25}Mg(p,γ)^{26}Al and ^{26}Al(p,γ)^{27}Si reaction rates. These rates affect the yield of ^{26}Al, which is one of the isotopes where the detailed and the synthetic models disagree most. We found that the ranges obtained by the detailed models are very close to those obtained by the synthetic models. More details are given in Sect. 4. For the other isotope where the detailed and the synthetic models disagree most, ^{21}Ne, we did not do the same exercise because the abundance is too low to make this isotope important, and there are no uncertainties on it derived from the reaction rates (see Sect. 4).

3. The choice of reaction rates and their uncertainties

The rate references, stellar energy windows and uncertainties are presented in Table 3. The bulk of the rates and their uncertainties come from the compilation of Iliadis et al. (2001), except for the ^{23}Na+p rates which come from the more recent work of Rowland et al (2004). The uncertainty ranges and stellar energy windows are for the range of temperatures relevant to the activation of the NeNa and MgAl chains during HBB: $70-100 \times 10^6$ K. The uncertainties are expressed as multiplication and division factors of the recommended rates to obtain the upper and the lower limits of the rates, respectively. The uncertainty ranges of Col. 4 describe in details how the uncertainty varies in the given range of temperature. The actual uncertainty ranges used in our calculations have been derived as the maximum values from Col. 4 and are listed in Col. 5. For the ^{20}Ne(p,γ)^{21}Na, ^{21}Ne(p,γ)^{22}Na, ^{23}Na(p,α)^{20}Ne, ^{24}Mg(p,γ)^{25}Al, ^{25}Mg(p,γ)^{26}Al reactions the uncertainty factors are approximately constant in the HBB temperature range, thus taking constant factors is a good description. We have checked that this is true by running the detailed $M = 6$ $M_\odot$, $Z = 0.02$ and $Z = 0.004$ models using a more accurate description of the upper limit of the ^{25}Mg(p,γ)^{26}Al rate and obtained the same results as described in Sect. 4 within 7%. For the reactions for which the uncertainty factors are not approximately constant we discuss at the end of Sect. 4.2 if our choice of the uncertainty range make the results less reliable.

The largest reaction rate uncertainties, up to three orders of magnitude, are associated with the ^{22}Ne(p,γ)^{23}Na and ^{26}Al(p,γ)^{27}Si rates. They are caused by contributions from as yet unobserved low-energy resonances. We expect these rate uncertainties to have the largest impact on the yields. Other well determined reaction rates, such as the ^{24}Mg(p,γ)^{25}Al rate, are not expected to have a large effect on the stellar yields.

To each value of the rate in between the lower and the upper limits a probability has to be assigned. Ideally, having available all the information on nuclear properties to calculate the rates, it would be appropriate to use a log-normal distribution (see Thompson & Iliadis 1999). However, there are two problems with this. First, for many rates the uncertainty ranges are very asymmetrical even on a logarithmic scale. Second, we already pointed out that the large rate uncertainties at relatively low temperatures are caused by as yet unobserved low-energy resonances. The rates are in such cases obtained in the following way (Angulo et al. 1999; Iliadis et al. 2001): (i) a maximum possible contribution is estimated – based on theoretical models or measured upper limits for the resonance strengths – for all threshold states; the inclusion of this contribution provides the

Table 2. Control values for the yields computed with the synthetic rapid code (first line for each model, e.g. 7.118e-03 stands for 7.118×10^{-3}) and with the detailed models (second line for each model, in italics). The ratio between the two is presented in the third line for each model.

Mass, metallicity	^{20}Ne	^{21}Ne	^{22}Ne	^{23}Na	^{24}Mg	^{25}Mg	^{26}Mg	^{26}Al	^{27}Al
5,0.02	7.118e-03	1.223e-05	1.771e-03	2.234e-04	2.231e-03	4.661e-04	7.541e-04	8.252e-07	2.646e-04
	6.681e-03	*1.965e-05*	*1.390e-03*	*2.291e-04*	*2.107e-03*	*3.431e-04*	*4.388e-04*	*4.966e-07*	*2.477e-04*
	1.06	0.62	1.27	0.98	1.06	1.36	1.72	1.66	1.07
6,0.02	8.770e-03	2.237e-06	2.047e-03	2.711e-04	2.690e-03	6.990e-04	1.040e-03	1.172e-05	3.373e-04
	8.211e-03	*1.067e-06*	*1.534e-03*	*3.012e-04*	*2.557e-03*	*4.817e-04*	*6.383e-04*	*4.096e-06*	*3.128e-04*
	1.07	2.09	1.33	0.90	1.05	1.45	1.63	2.86	1.08
5,0.008	2.974e-03	1.463e-06	2.175e-03	8.740e-05	8.445e-04	6.275e-04	8.250e-04	2.085e-05	1.488e-04
	2.678e-03	*5.437e-07*	*2.379e-03*	*1.202e-04*	*7.861e-04*	*4.307e-04*	*6.922e-04*	*8.961e-06*	*1.284e-04*
	1.11	2.69	0.91	0.73	1.07	1.46	1.19	2.32	1.16
6,0.008	3.604e-03	1.213e-06	1.852e-03	7.352e-05	5.878e-04	1.044e-03	9.582e-04	1.037e-04	1.855e-04
	3.289e-03	*4.463e-07*	*1.233e-03*	*1.072e-04*	*6.711e-04*	*6.929e-04*	*6.389e-04*	*2.527e-05*	*1.430e-04*
	1.10	2.72	1.50	0.69	0.88	1.51	1.40	4.10	1.30
5,0.004	1.555e-03	1.569e-06	2.576e-03	4.908e-05	3.544e-04	7.456e-04	1.184e-03	5.012e-05	1.007e-04
	1.360e-03	*5.780e-07*	*2.371e-03*	*9.156e-05*	*3.390e-04*	*4.934e-04*	*9.944e-04*	*1.469e-05*	*8.363e-05*
	1.14	2.71	1.09	0.54	1.04	1.51	1.19	3.41	1.20
6,0.004	1.830e-03	1.108e-06	1.374e-03	2.553e-05	5.730e-05	8.156e-04	8.629e-04	1.652e-04	1.526e-04
	1.664e-03	*3.338e-07*	*9.963e-04*	*4.506e-05*	*6.782e-05*	*6.999e-04*	*7.182e-04*	*5.223e-05*	*9.631e-05*
	1.10	3.32	1.38	0.57	0.84	1.16	1.20	3.16	1.58
4,0.0001	1.741e-04	1.563e-06	4.047e-03	3.254e-05	1.766e-05	4.121e-04	1.684e-03	1.478e-04	4.297e-05
	2.156e-04	*8.663e-07*	*3.697e-03*	*1.315e-04*	*3.578e-05*	*4.864e-04*	*1.664e-03*	*2.747e-05*	*1.214e-04*
	0.81	1.80	1.09	0.25	0.49	0.85	1.01	5.38	0.35
5,0.0001	2.436e-04	1.515e-06	3.128e-03	3.703e-05	3.772e-05	5.271e-04	2.107e-03	5.038e-05	1.489e-04
	1.642e-04	*3.878e-07*	*3.088e-03*	*9.655e-05*	*3.010e-05*	*5.799e-04*	*2.110e-03*	*2.333e-05*	*1.077e-04*
	1.48	3.91	1.01	0.38	1.25	0.91	1.00	2.16	1.38
6,0.0001	2.146e-04	8.538e-07	1.888e-03	2.474e-05	5.588e-06	3.674e-04	1.373e-03	4.399e-05	1.716e-04
	6.973e-05	*1.461e-08*	*3.423e-04*	*8.766e-06*	*1.268e-06*	*8.058e-05*	*2.667e-04*	*6.145e-06*	*3.211e-05*
	3.08	58.4	5.51	2.82	4.40	4.56	5.15	7.16	5.34

Table 3. References and uncertainties (in the range $T = 70-100 \times 10^6$ K) for the considered reaction rates.

Rate	Energy[a] (keV)	Reference	Uncertainty	Chosen uncertainty
^{20}Ne$(p,\gamma)^{21}$Na	67–157	Iliadis et al. (2001) = NACRE	/2, ×1.5	/2, ×1.5
^{21}Ne$(p,\gamma)^{22}$Na	67–157	Iliadis et al. (2001)	/1.25, ×1.20	/1.25, ×1.20
^{22}Ne$(p,\gamma)^{23}$Na	67–157	Iliadis et al. (2001) = Hale et al. (2002)	/1.43 to /2, ×982 to ×1888	/2, ×2000
^{23}Na$(p,\gamma)^{24}$Mg	73–166	Rowland et al. (2004)	/5 to /40, ×7.8 to ×9.8	/40, ×10
^{23}Na$(p,\alpha)^{20}$Ne	73–166	Rowland et al. (2004)	/1.3, ×1.3	/1.3, ×1.3
^{24}Mg$(p,\gamma)^{25}$Al	78–175	Iliadis et al. (2001) = Powell et al. (1999)	/1.2, ×1.2	/1.2, ×1.2
^{25}Mg$(p,\gamma)^{26}$Al	78–175	Iliadis et al. (2001)	/2, ×1.5	/2, × 1.5
^{26}Mg$(p,\gamma)^{27}$Al	78–175	Iliadis et al. (2001)	/1.4 to /4.2, ×4.1 to ×8.9	/4, ×10
^{26}Al$_{ground}(p,\gamma)^{27}$Si	83–184	Iliadis et al. (2001)	/1.25 to /2, ×11. to ×572	/2, ×600
^{27}Al$(p,\gamma)^{28}$Si	83–184	Iliadis et al. (2001)	/1.25, ×1.2 to ×2.8	/1.25, ×3

[a] Effective stellar energy window for the reaction, calculated as $(E_0 - \Delta/2)_{70 \text{ MK}}$ - $(E_0 + \Delta/2)_{100 \text{ MK}}$, where E_0 is the location of the Gamow peak and Δ is its $1/e$ width.

upper total rate limit; (ii) disregarding any contributions from the threshold states provides the lower total rate limit; and (iii) the recommended total rates are then arrived at by multiplying the upper limit contributions of the threshold states by an (arbitrary) factor of 0.1. It should be clear from this description that there is no straightforward manner for representing the reaction rate errors by a meaningful probability distribution function. For these reasons, we have decided to assign the same probability to each value of the rates between the upper and the lower limits, i.e. to use a flat probability distribution. The choice of a probability distribution does not influence our resulting ranges of uncertainty in the yields, which remain a strong result of our work. However, it defines how the yield values are distributed, and hence, for example, which is the most probable value of the

distribution associated with each yield. In Sect. 4.2 we present two examples of the probability distribution of the yields that we obtain, keeping in mind that, while assigning a probability distribution to the rates is still difficult, these examples should be only considered as test exercises.

4. Results

Tables 4 to 12 present the range of uncertainties we obtain for the Ne, Na, Mg and Al isotopes when varying the reaction rates within their uncertainty ranges. Only variations of more than 10% are listed. In each table we present yield variations relative to the control value (see Table 2) as functions of the stellar model (Col. 1: mass in $M_\odot$ and metallicity) and of the reaction

Table 4. Multiplication factors for the ^{20}Ne yields.

Model	^{22}Ne$(p,\gamma)^{23}$Na	All reactions
5,0.004	1.0–1.11	0.99–1.15
6,0.004	1.0–1.25	0.98–1.29
4,0.0001	1.0–1.46	1.0–1.60
5,0.0001	0.95–5.50	0.93–6.20
6,0.0001	0.93–4.34	0.90–4.75

Table 5. Multiplication factors for the ^{21}Ne yields.

Model	All reactions
6,0.0001	1.0–1.11

Table 6. Multiplication factors for the ^{22}Ne yields.

Model	^{22}Ne$(p,\gamma)^{23}$Na	All reactions
5,0.02	0.83–1.0	0.83–1.0
6,0.02	0.33–1.0	0.33–1.0
5,0.008	0.20–1.0	0.20–1.0
6,0.008	0.18–1.0	0.18–1.01
5,0.004	0.18–1.0	0.18–1.0
6,0.004	0.17–1.01	0.17–1.02
4,0.0001	0.17–1.0	0.17–1.0
5,0.0001	0.14–1.01	0.14–1.01
6,0.0001	0.17–1.01	0.17–1.01

rates (headers). The last column gives the range of uncertainties we obtain when we vary all the reaction rates simultaneously in all possible combinations of lower and upper limits. The uncertainties in the yields obtained when varying simultaneously all the reaction rates are larger than those obtained by vary each single rate since in this case the uncertainties from all rates are applied, however, they do not always correspond simply to multiplying the factors obtained by varying each single rate. This indicates the complex interplay of the reactions involved in the NeNa and MgAl chains, and points out the importance of computing models using all possible combinations of rates.

The isotope least affected by reaction-rate uncertainties is ^{21}Ne, which is also typically destroyed by HBB and thus has very low stellar yields. All the other isotopes show important variations in their yields, which of course increase in magnitude with increasing the HBB efficiency. This is mostly determined by the temperature at the base of the convective envelope, which increases with decreasing metallicity and increasing stellar mass (Table 1). Thus, the rate uncertainties typically have a larger impact on models of higher masses and lower metallicities. On the other hand, the TDU mass is also an important parameter in determining the HBB efficiency, as it feeds fresh ^{22}Ne, ^{25}Mg and ^{26}Mg nuclei from the He intershell into the envelope to be burned by the NeNa and MgAl chains. The TDU mass increases with decreasing the metallicity, but, contrary to the HBB temperature, it typically decreases with increasing the stellar mass in IM-AGB models (Table 1). The combined effect of TDU mass and HBB temperature eventually determines the HBB efficiency and hence the effect of the rate uncertainties. For example, the uncertainty range of ^{23}Na increases with decreasing the metallicity (Table 7), however, it decreases with the stellar mass at any given metallicity lower than solar, because less TDU means less ^{22}Ne from the He intershell to be burned into ^{23}Na in the envelope.

Table 7 also illustrates that the yields of ^{23}Na suffer from large uncertainties, up to two orders of magnitudes. While the upper range uncertainties are only due to the large uncertainty of the ^{22}Ne$(p,\gamma)^{23}$Na reaction rate, the lower range uncertainties are also determined by the effect of uncertainties in the ^{23}Na$+p$ reaction rates. Neon-22 is an important product of IM-AGB stars, with yields of the order of 10^{-3} $M_\odot$ in all our models (see Table 2). Table 6 shows that these numbers are very much affected by the large uncertainties associated with the ^{22}Ne$(p,\gamma)^{23}$Na reaction rate, as yields down to 0.14 of the control values are within the uncertainties. The large initial abundance of ^{20}Ne is almost unchanged during the AGB evolution and galactic production of this α-nucleus is dominated by supernova nucleosynthesis. A small but interesting range of variation, up to a factor of $\simeq 6$, affects the yield of this isotope (Table 4). This uncertainty is mostly due, again, to the effect of the large uncertainty of the ^{22}Ne$(p,\gamma)^{23}$Na reaction combined with the feedback from the ^{23}Na$(p,\alpha)^{20}$Ne rate. We note that the NACRE rate for the ^{22}Ne$(p,\gamma)^{23}$Na reaction is about three orders of magnitude higher than the current recommended value in the HBB temperature range. Thus, model calculations performed using the NACRE rate would roughly correspond to taking our lower limit for the ^{22}Ne and upper limit for the ^{23}Na and ^{20}Ne yields.

The same rate also affects the yield of ^{24}Mg, with yield variations up to a factor $\simeq 5$. However, for this isotope much larger multiplication factors, up to 48, only appear when all rates are simultaneously changed, and cannot be obtained by simply multiplying the uncertainties produced by each rate. This is because of the combined effect of the uncertainties of two reactions, ^{22}Ne$(p,\gamma)^{23}$Na and ^{23}Na$(p,\gamma)^{24}$Mg. Taking the upper limits for these two rates we find, for the 5 $M_\odot$, $Z = 0.0001$ model, a multiplication factor of 38, close to that obtained by varying all the rates.

The most uncertain isotope produced by the MgAl chain is ^{26}Al. The yield of this radioactive isotope is very high in some of our models, reaching $\simeq 10^{-5}$ $M_\odot$. However, the large uncertainty associated with the rate of its destruction reaction, ^{26}Al$(p,\gamma)^{27}$Si, makes it possible also to have almost *no* production of this isotope in any of our models. The very large upper limit for this rate should be tested against observational constraints, such as the ^{26}Al/^{27}Al ratio obtained in presolar silicon carbide and oxide grains. It is interesting to note that the range of uncertainty of the upper limit of ^{25}Mg$(p,\gamma)^{26}$Al reaction rate is relatively small but is almost completely reflected in the corresponding variations of the ^{26}Al yield. In summary, the ^{26}Al yield can be multiplied by factors down to 0.02, but also multiplied by factors up to 3. The yield of ^{25}Mg itself, instead, does not feel the uncertainty of the ^{25}Mg$(p,\gamma)^{26}$Al reaction rate as strongly, but rather varies significantly, up to a factor of 1.7, only when all the rates are simultaneously changed. Finally, ^{26}Mg mostly feels the uncertainties in the ^{26}Mg$(p,\gamma)^{27}$Al rate, while ^{27}Al is affected by the uncertainties connected to both the ^{26}Mg$(p,\gamma)^{27}$Al and ^{26}Al$(p,\gamma)^{27}$Si rates, with multiplication factors ranging up to 6 and down to 0.39.

4.1. Interdependencies of the yields

To provide uncertainty ranges as given in Tables 4 to 12 is not enough if one wants to test these errors, for example by including them in GCE models. In fact, the yield variations are correlated to each other so that it is not possible to freely pick any combination of upper and/or lower limits for each isotope. Instead, to produce consistent model predictions one should test, for example, the upper limit of the ^{22}Ne yield together with the

Table 7. Multiplication factors for the ^{23}Na yields.

Model	^{22}Ne$(p,\gamma)^{23}$Na	^{23}Na$(p,\gamma)^{24}$Mg	^{23}Na$(p,\alpha)^{20}$Ne	All reactions
5,0.02	1.–2.41			1.–2.41
6,0.02	1.–6.21			0.97–6.25
5,0.008	0.95–21.3			0.91–21.5
6,0.008	0.89–17.9	0.86–1.02	0.90–1.09	0.68–19.3
5,0.004	0.80–41.6			0.70–42.8
6,0.004	0.67–26.7	0.80–1.03	0.83–1.18	0.43–30.9
4,0.0001	0.62–106.3			0.61–107.2
5,0.0001	0.53–41.3	0.86–1.02	0.88–1.12	0.41–46.8
6,0.0001	0.56–32.6	0.86–1.02	0.87–1.13	0.47–36.5

Table 8. Multiplication factors for the ^{24}Mg yields.

Model	^{22}Ne$(p,\gamma)^{23}$Na	^{23}Na$(p,\gamma)^{24}$Mg	^{24}Mg$(p,\gamma)^{25}$Al	All reactions
6,0.008			0.89–1.10	0.89–1.34
5,0.004				0.96–1.37
6,0.004	0.99–1.24		0.73–1.40	0.72–4.09
4,0.0001	1.–1.41			0.99–5.11
5,0.0001	0.94–5.27	0.88–1.94		0.81–48.0
6,0.0001	0.98–2.20	0.95–1.37		0.91–14.3

Table 9. Multiplication factors for the ^{25}Mg yields.

Model	^{25}Mg$(p,\gamma)^{26}$Al	All reactions
6,0.008		0.90–1.16
6,0.004	0.90–1.12	0.90–1.25
5,0.0001		0.94–1.67
6,0.0001		0.93–1.66

Table 10. Multiplication factors for the ^{26}Mg yields.

Model	^{26}Mg$(p,\gamma)^{27}$Al	All reactions
6,0.008	0.80–1.02	0.78–1.03
5,0.004	0.88–1.01	0.87–1.01
6,0.004	0.72–1.04	0.69–1.06
5,0.0001	0.73–1.03	0.72–1.05
6,0.0001	0.65–1.06	0.65–1.07

Table 11. Multiplication factors for the ^{26}Al yields. In italics are the variations derived by running the corresponding detailed models.

Model	^{25}Mg$(p,\gamma)^{26}$Al	^{26}Al$(p,\gamma)^{27}$Si	All reactions
5,0.02	0.81–1.19		0.80–1.19
6,0.02	0.56–1.44 (*1.34*)	0.46 (*0.43*)–1.0	0.27–1.46
5,0.008	0.52–1.47	0.36–1.0	0.18–1.48
6,0.008	0.52–1.44	0.07–1.02	0.04–1.61
5,0.004	0.52–1.44	0.14–1.01	0.07–1.51
6,0.004	0.55–1.38 (*1.35*)	0.02 (*0.03*)–1.07	0.01–1.70
4,0.0001	0.51–1.46	0.38–1.0	0.20–1.47
5,0.0001	0.53–1.41	0.03–1.07	0.02–2.70
6,0.0001	0.56–1.36	0.03–1.16	0.02–3.03

lower limit of the ^{23}Na yield and so on. In Table 13, available in electronic form at the CDS, we provide complete results for a relatively small subset of models obtained by varying only the six most uncertain reactions between their upper and lower limits. Moreover, we have prepared a web-interface program located at http://www.astro.uu.nl/~izzard/cgi-bin/varyrates.cgi through which it is possible to perform calculations for any synthetic stellar model presented in this paper changing any of the rates.

4.2. Yield probability distribution

As discussed in Sect. 3, due to the difficulty of attributing a statistical significance to the estimates of upper and lower limits, we employed a flat probability distribution for the rates. In this section we show that the resulting yield distributions do not necessarily follow the rate distribution, i.e. they are not always flat. The following examples should only be considered as test exercises, and we report them in order to illustrate the future potential of our method in estimating yield distributions, and hence recommended values and uncertainties for the yields.

We show two examples calculated for the 5 $M_\odot$ $Z = 0.008$ model. The first yield distribution is that which we obtain for ^{26}Al when varying the ^{25}Mg$(p,\gamma)^{26}$Al reaction rate. As shown in Fig. 1 (left panel) this is a simple situation in which the variation in the ^{26}Al yield is linearly dependent on the variation of the ^{25}Mg$(p,\gamma)^{26}$Al reaction rate. The resulting yield distribution is shown in Fig. 1 (right panel) and is almost flat, with the same number of stars (within 5%) reproducing the different yield ranges, represented by the bins. A more interesting example concerns the variation of ^{23}Na as function of the ^{22}Ne$(p,\gamma)^{23}$Na reaction rate. The variation of the yield in this case is *not* linearly dependent on the variation of the ^{22}Ne$(p,\gamma)^{23}$Na reaction rate (Fig. 2, left panel). When the rate is slow, the reaction approaches equilibrium and the yield of ^{23}Na increases linearly with the rate. As the rate becomes faster, the yield of ^{23}Na stops its rapid rise because almost all the ^{22}Ne fuel is used up. The ^{23}Na/^{22}Ne ratio is nearly at its equilibrium value, but the amount of extra mass converted to ^{23}Na as a result of the increased rate is small because there is simply no more ^{22}Ne fuel. This is complicated because the third dredge up replenishes the supply of ^{22}Ne and allows some extra ^{23}Na to be produced. This leads to the shallow slope at high rates. Note that ^{22}Ne is always produced during the final few pulses when the temperature at the base of the convective envelope falls below that required to activate the ^{22}Ne$(p,\gamma)^{23}$Na reaction. Consequently, the ^{23}Na yield distribution leans towards high values, around $\simeq 20$ of the multiplication

Table 12. Multiplication factors for the ^{27}Al yields. In italics are the variations derived by running the corresponding detailed models.

Model	^{26}Mg$(p, \gamma)^{27}$Al	^{26}Al$(p, \gamma)^{27}$Si	All reactions
6,0.02	0.99–1.12		0.99–1.15
5,0.008	0.97–1.36	1.0–1.12	0.97–1.54
6,0.008	0.88–2.09	0.99–1.65	0.87–3.14
5,0.004	0.86–2.46	1.0–1.58	0.85–3.32
6,0.004	0.78–2.63	0.91–2.29 (*1.59*[a])	0.62–4.78
4,0.0001	0.79–3.38	1.0–1.31	0.78–3.85
5,0.0001	0.48–4.97	0.97–1.43	0.43–6.15
6,0.0001	0.47–3.91	0.95–1.29	0.39–4.88

[a] This result from the detailed model is closer to what expected by a comparison to models of other masses and metallicities. We do not yet have a ready explanation for the 44% higher range shown by the synthetic model.
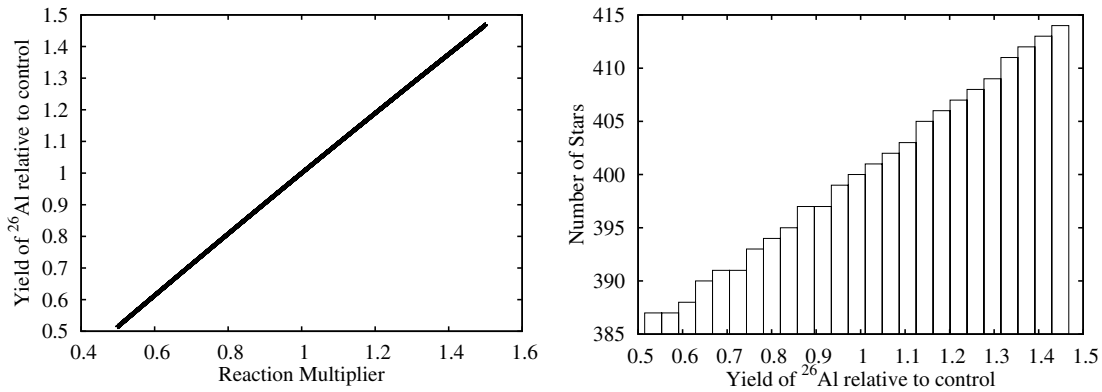
Fig. 1. For the 5 $M_\odot$ $Z = 0.008$ model we show *(left)*: the multiplication factor for ^{26}Al as a function of the variation factor of the ^{25}Mg$(p, \gamma)^{26}$Al reaction rate, *(right)*: the number of models obtained for each bin representing a yield interval.
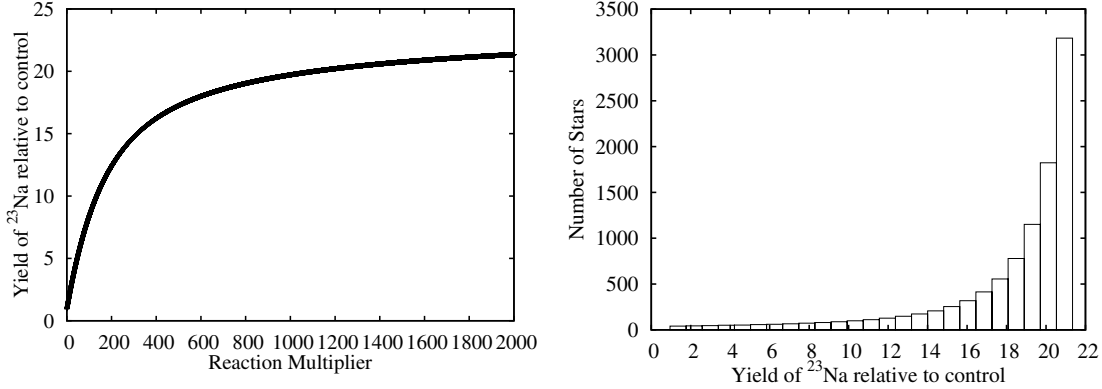
Fig. 2. For the 5 $M_\odot$ $Z = 0.008$ model we show *(left)*: the multiplication factor for ^{23}Na as a function of the variation factor of the ^{22}Ne$(p, \gamma)^{23}$Na reaction rate, *(right)*: the number of models obtained for each bin representing a yield interval.

factor, and these values are more likely to occur than smaller values (Fig. 2, right panel). This is a consequence of the fact that we have chosen a flat distribution to represent the rate uncertainties. We stress again that this choice is still quite arbitrary, and these yield distributions are test exercises. We cannot give recommendations on the most likely value or the standard deviation from the yield distributions and we suggest, for the time being, all the values that we obtain for each yields to be equally probable.

The left panel of Fig. 2 is also useful to demonstrate that our choice of a constant value of 2000, instead of the actual range of 982 to 1888, for the upper limit factor of the ^{22}Ne$(p, \gamma)^{23}$Na rate does not affect the accuracy of the results, since the results do not change once the rate is multiplied by more than 800. For the ^{26}Al$(p, \gamma)^{27}$Si rate our results show that, similarly to the case of ^{23}Na discussed above, the effect of varying this rate are more

or less the same once the rate has been multiplied by a factor $\simeq 200$ because for this value of the rate all ^{26}Al is consumed and the yield distribution is weighed towards the low ^{26}Al yields. However, contrarily to the case of the ^{22}Ne$(p, \gamma)^{23}$Na rate discussed above, the upper limit of the ^{26}Al$(p, \gamma)^{27}$Si rate ranges below this saturation value, hence we should take the results obtained changing this rate as maximum possible ranges. We have tested this point by running the detailed $M = 6$ $M_\odot$ $Z = 0.02$ and $Z = 0.004$ models using the proper upper limit for the ^{26}Al$(p, \gamma)^{27}$Si rate, i.e. including an accurate description of its variation with the temperature and found that in fact the ranges of variation are smaller than those reported in Table 11: 0.67 rather than 0.43 for the $Z = 0.02$ model, and 0.19 rather than 0.02 for the $Z = 0.004$ model. For ^{27}Al, instead, the ranges of variation are unchanged: 1.47 rather than 1.59 for the $Z = 0.004$

model. The same point holds for the lower limit of this rate. The same problem arises for the $^{26}Mg(p, \gamma)^{27}Al$ reaction, whose uncertainty factors (Table 3) also vary significantly with the temperature. Thus, we should consider also the yield variations obtained varying this rate as the maximum allowed. For the $^{23}Na(p, \gamma)^{24}Mg$ reaction, the lower limit of the rate shows a large range of variations. However, our results show that the uncertainty associated with the lower limit of this rate does not affect any isotope to more than 20%. Finally, for the $^{27}Al(p, \gamma)^{28}Si$ reaction our results have showed that changes in this rate do not affect any isotopic yield. This result was confirmed by a detailed $M = 6\ M_\odot\ Z = 0.02$ model computed using the upper limit of the rate. In summary, only the results obtained by varying the $^{26}Mg(p, \gamma)^{27}Al$ and the $^{26}Al(p, \gamma)^{27}Si$ reactions should be taken as the maximum allowed.

5. Summary and conclusions

We have shown that uncertainties in the yields of the Ne, Na, Mg and Al isotopes are present in connection to proton-capture reaction rates. The most uncertain rates are those of the $^{26}Al(p, \gamma)^{27}Si$ and the $^{22}Ne(p, \gamma)^{23}Na$ reactions, with variations up to 3 orders of magnitude. The $^{22}Ne(p, \gamma)^{23}Na$ uncertainties produce huge variations, up to two orders of magnitude, in the yields of ^{22}Ne and ^{23}Na, as well as uncertainties up to a factor of 5 in the yields of ^{20}Ne and ^{24}Mg. The $^{26}Al(p, \gamma)^{27}Si$ uncertainties lead to large variations, up to two orders of magnitude, in the yields of ^{26}Al. The yield of ^{24}Mg is also affected by the uncertainty in the $^{23}Na(p, \gamma)^{24}Mg$ rate, with strong effects appearing when this rate is considered together with the $^{22}Ne(p, \gamma)^{23}Na$ rate. The effect of the relatively small uncertainty of the $^{25}Mg(p, \gamma)^{26}Al$ reaction rate turned out to be quite important because it is completely, and not only partially as for the other rates, reflected in the uncertainty of the ^{26}Al yields. Finally, the $^{26}Mg(p, \gamma)^{27}Al$ affects the yields of both ^{26}Mg and ^{27}Al. In summary, to obtain more reliable Ne, Na, Mg and Al yields from IM-AGB stars the rates to be better determined are: $^{22}Ne(p, \gamma)^{23}Na$, $^{23}Na(p, \gamma)^{24}Mg$, $^{25}Mg(p, \gamma)^{26}Al$, $^{26}Mg(p, \gamma)^{27}Al$, and $^{26}Al(p, \gamma)^{27}Si$.

It is difficult to predict a priori exactly what will be the impact of our uncertainty ranges and detailed models should be constructed to address each of the observational constraints related to HBB nucleosynthesis. With regards to globular cluster anomalies, the Na abundances predicted by Fenner et al. (2004) to be too large to match the observed abundances correspond to the upper limits of the Na yields and a revision of this point is necessary. On the other hand, the predicted too high Mg abundances may be more difficult a problem to solve taking into account reaction rate uncertainties, while the observed high Al abundances may also be matched within uncertainties. Only performing detailed calculations will it be possible to verify if a solution for globular cluster anomalies is feasible within the uncertainties we have presented here.

References

Angulo, C., Arnould, M., Rayet, M., et al. 1999, Nucl. Phys. A, 656, 3 (NACRE)
Ashenfelter, T. P., Mathews, G. J., & Olive, K. A. 2004, ApJ, 615, 82
Boothroyd, A. I., Sackmann, I.-J., & Ahern, S. C. 1993, ApJ, 416, 762
Caughlan, G. R., & Fowler, W. A. 1988, Atom. Data Nucl. Data Tables, 40, 283
Fenner, Y., Campbell, S., Karakas, A. I., Lattanzio, J. C., & Gibson, B. K. 2004, MNRAS, 353, 789
Fenner, Y., Murphy, M. T., & Gibson, B. K. 2005, MNRAS, 358, 468
Frost, C. A., Lattanzio, J. C., & Wood, P. R. 1998, ApJ, 500, 355
García-Hernández, D. A., García-Lario, P., Plez, B., et al. 2007, A&A, 462, 711
Gratton, R., Sneden, C., & Carretta, E. 2004, ARA&A, 42, 385
Hale, S. E., Champagne, A. E., Iliadis, C., et al. 2002, Phys. Rev. C, 65, 015801
Herwig, F. 2005, ARA&A, 43, 435
Herwig, F., & Austin, S. M. 2004 ApJ, 613, L73
Iliadis, C., D'Auria, J. M., Starrfield, S., Thompson, W. J., & Wiescher, M. 2001, ApJS, 134, 151
Iliadis, C., Champagne, A., José, J., Starrfield, S., & Tupper, P. 2002, ApJS, 142, 105
Izzard, R. G., Dray, L. M., Lugaro, M., Karakas, A. I., & Tout, C. A. 2006, A&A, 460, 565
Izzard, R. G., Tout, C. A., Karakas, A. I., & Pols, O. R. 2004, MNRAS, 350, 407
Karakas, A. I., Lattanzio, J. C., & Pols, O. R. 2002, PASA, 19, 515
Karakas, A. I., Lugaro, M., Wiescher, M., Goerres, J., & Ugalde, C. 2006, ApJ, 643, 471
Lugaro, M., Karakas, A. I., Nittler, L. R., et al. 2007, A&A, 461, 657
Lugaro, M., Ugalde, C., Karakas, A. I., Görres, J., Wiescher, M., Lattanzio, J. C., & Cannon, R. C. 2004, ApJ, 615, 934
Mazzitelli, I., D'Antona, F., & Ventura, P. 1999, A&A, 348, 846
Peimbert, M. 1980, in Physical processes in Red Giants, ed. I. Iben, & A. Renzini (Dordrecht: Reidel), 409
Plez, B., Smith, V. V., & Lambert, D. D. 1993, ApJ, 418, 812
Pottasch, S. R., & Bernard-Salas, J. 2006, A&A, 457, 189
Powell, D. C., Iliadis, C., Champagne, A. E., et al. 1999, Nucl. Phys. A, 660, 349
Rowland, C., Iliadis, C., Champagne, A. E., et al. 2004, ApJ, 615, L7
Spite, M., Cayrel, R., Plez, B., et al. 2005, A&A, 430, 655
Stanghellini, L., Guerrero, M. A., Cunha, K., Manchado, A., & Villaver, E. 2006, ApJ, 651, 898
Stoesz, J. A., Herwig, F. 2003, MNRAS, 340, 763
Thompson, & Iliadis C. 1999, Nucl. Phys. A647, 259
Ventura, P., & D'Antona, F. 2005a, A&A, 439, 1075
Ventura, P., & D'Antona, F. 2005b, A&A, 431, 279
Ventura, P., & D'Antona, F. 2006, A&A, 457, 995
Wood, P. R., Bessel, M.S., & Fox, M. W. 1983, ApJ, 272, 99